

Cold gas in the intracluster medium: implications for flow dynamics and powering optical nebulae

Edward C. D. Pope[★], Thomas W. Hartquist and Julian M. Pittard

School of Physics & Astronomy, University of Leeds, Leeds LS2 9JT

Accepted 2008 June 20. Received 2008 June 20; in original form 2008 January 30

ABSTRACT

We show that the mechanical energy-injection rate generated as the intracluster medium (ICM) flows around cold clouds may be sufficient to power the optical and near-infrared emission of nebulae observed in the central regions of a sample of seven galaxy clusters. The energy-injection rate is extremely sensitive to the velocity difference between the ICM and cold clouds, which may help to explain why optical and infrared luminosity is often larger than expected in systems containing active galactic nuclei. We also find that mass recycling is likely to be important for the dynamics of the ICM. This effect will be strongest in the central regions of clusters where there is more than enough cold gas for its evaporation to contribute significantly to the density of the hot phase.

Key words: hydrodynamics – galaxies: active – cooling flows.

1 INTRODUCTION

Line-emitting nebulae surround approximately a third of all Brightest Cluster Galaxies (BCGs) (Crawford et al. 1999). The occurrence of these optical nebulae appears to have some correspondence to the short radiative cooling time of the cluster. Nearby examples, such as NGC 1275, in Perseus, NGC 4696 in Centaurus, and A1795, show extended filamentary structures up to 50 kpc from the central galaxy (see Hatch, Crawford & Fabian 2007, and references therein). Many of these BCGs also contain reservoirs of 10^8 – $10^{11.5} M_{\odot}$ of molecular hydrogen (e.g. Edge 2001).

One of the prevalent emission lines in these nebulae is $[\text{N II}]\lambda 6584$. Since $[\text{N II}]$ is collisionally excited by thermal electrons, this line measures the heating rate in the gas, whereas the $\text{H}\alpha$ line measures the ionization rate (Donahue & Voit 1991). A large heating rate compared to the ionization rate leads to large $[\text{N II}]/\text{H}\alpha$ and $[\text{O II}]/\text{H}\alpha$ ratios. To date, the power source remains unknown, although numerous heating processes have been investigated. These include ionization by the central active galactic nucleus (AGN), ionization by hot young stars, heating by X-rays from the intracluster medium (ICM), conduction of heat from the ICM (Donahue et al. 2000) and turbulent mixing layers (Crawford & Fabian 1992). Cosmic rays, preferentially diffusing along the magnetic field lines trailing behind rising bubbles, could possibly drive the excitation in those filaments that are located in bubble wakes (Ruszkowski et al. 2007). However, there are problems associated with each possibility listed above (see Hatch et al. 2006). As a consequence, the nature of the power source(s) remains unknown.

Energy dissipation due to drag has, so far, not been considered as a potential source of energy for the filaments. In principle, dissipation

by drag could be responsible for at least the heating of the optically emitting gas, and thus the $[\text{N II}]$ emission, if not the $\text{H}\alpha$ emission.

Recent numerical simulations suggest that the filamentary structures can be formed by an outflow stripping material from cold clouds (Pope et al. 2008). These filaments only become long if the wind is sufficiently fast. The kinematics and morphology also suggest that the filaments may be many tens of Myr old. Dissipation due to drag would necessarily occur all along the filament and would provide a spatially distributed source of energy that could power the optical emission.

So far the presence of vast quantities of cold material has been ignored in most numerical simulations of the diffuse gas in galaxy clusters. This is partly due to the difficulty of implementing a cold phase in such simulations, but also because the importance of its presence has not been hitherto established. The effect of a cold phase may not be entirely negligible. In fact, the presence of significant quantities of cold gas might alter the flow dynamics in the central regions of galaxy clusters. This could occur through the addition of mass, stripped from cold clouds, or energy and momentum transfer associated with the mass loss from the clouds.

In this article, we estimate mass transfer parameters for a sample of galaxy clusters: Virgo, Perseus, Hydra, A2597, A2199, A1795 and A478. We also investigate drag as a possible power source for the optical emission of these nebulae. In Section 2, we discuss the constraints on cloud properties. In Section 3, we concentrate on the significance of mass transfer between the phases. Section 4 focuses on mechanical energy as a power source for the optical emission, and we summarize in Section 5.

2 CONSTRAINTS ON COLD CLOUDS

There is little direct evidence constraining cloud sizes in the ICM. For example, if the optical filaments are drawn from cold clouds, the

[★]E-mail: e.c.d.pope@leeds.ac.uk

filaments are likely to be no wider than these clouds. However, the width of the filaments are usually constrained to be < 1 kpc which is not a very strong limit. Maps presented by Salomé et al. (2008) show clumpy structures in the CO emission. Given the spatial resolution of the technique, the upper limit on the sizes of these clumps is ~ 450 pc in the Perseus cluster. Such clumps may be complexes of giant molecular clouds, but it is difficult to tell.

In the simplest cloud formation scenario, there is a heat conduction length scale above which fluctuations are not stabilized and clouds form, which is given by Boehringer & Fabian (1989) (following Field 1965) as

$$\lambda > 6 \left(\frac{\eta}{0.01} \right)^{1/2} \left(\frac{T}{10^8 \text{ K}} \right)^{3/2} \left(\frac{n}{0.1 \text{ cm}^{-3}} \right)^{-1} \text{ kpc}, \quad (1)$$

where η is the thermal conduction suppression factor, T is the ambient temperature, and n is the number density of the gas. Equation (1) implies a minimum cloud mass of

$$M > 1.7 \times 10^8 \left(\frac{\eta}{0.01} \right)^{3/2} \left(\frac{T}{10^8 \text{ K}} \right)^{9/2} \left(\frac{n}{0.1 \text{ cm}^{-3}} \right)^{-2} M_{\odot}. \quad (2)$$

McKee & Cowie (1977) present a similar argument. equation (2) indicates that smaller, lower mass clouds can form near the central regions of galaxy clusters, where the gas density is at its highest. More massive clouds may form further out, where the density is lower.

However, the physics of the ICM is rather more complex than this description implies. Processes such as magnetic turbulence are likely to play roles, with η possibly as small as 10^{-6} . Consequently, clouds much smaller in mass than $10^8 M_{\odot}$ may form. Given the difficulty of observing single cold clouds, much of the work on cloud properties has relied on theoretical reasoning (e.g. Daines, Fabian & Thomas 1994; Loewenstein & Fabian 1990). However, there remains no clear picture of the mass and size of individual clouds. All we can say for certain is that, based on filament widths, and the CO data, the clouds are probably less than 0.5 kpc wide and there is likely to be a distribution of cloud sizes. Also, the cold mass should not be confused with the mass of optically emitting ionized material, which can be determined from the H α emission and is much less than the total quantity of cold gas.

If the most massive clouds are molecular, much of the cloud material may be at temperatures of tens of Kelvin. Pressure equilibrium with the surrounding X-ray emitting gas would imply a density of order 10^{-20} – 10^{-19} g cm $^{-3}$. A spherical cloud of $10^8 M_{\odot}$ would have a diameter of ~ 100 pc. Though the cloud mass is very uncertain, we will typically adopt values of 10^{-19} g cm $^{-3}$, 100 pc and $10^8 M_{\odot}$ for the density, diameter and mass where presenting numerical results. However, we will make the ways in which our results scale with the assumed values very clear.

2.1 The motion of clouds

The clouds will be referred to as the dispersed phase, while the intracluster gas will be referred to as the continuous phase denoted by subscripts d and c, respectively.

Concentrating only on drag, we can write the equation of motion of a cold cloud through the ICM as

$$m \frac{dv}{dt} = \frac{1}{2} C_D \frac{\pi D^2}{4} \rho_c (u - v) |u - v|, \quad (3)$$

where C_D is the drag coefficient, D is the diameter of the cloud, ρ_c is the density of the continuous phase, u is the speed of the continuous phase, and v is the speed of the dispersed phase.

Dividing both sides of equation (3) by the cloud mass and assuming that the cloud is spherical with uniform density, we find

$$\frac{dv}{dt} = \frac{(u - v)}{\tau_v}, \quad (4)$$

where

$$\tau_v = \frac{4D}{3C_D} \left(\frac{\rho_d}{\rho_c} \right) \frac{1}{|u - v|}. \quad (5)$$

Equations (4) and (5) mean that the cloud's motion can be described in terms of the drag coefficient. The drag coefficient is a function of the Reynolds number of the fluid flowing around an obstacle, and the Mach number (although for subsonic flows this effect is small). The Reynolds number is given by

$$Re = \frac{D \rho_c |u - v|}{\mu_c}, \quad (6)$$

where μ_c is the viscosity of the continuous phase. An approximate relation for the subsonic drag coefficient for flow past a solid object at $Re < 1000$ is given by Crowe, Sommerfeld & Tsuji (1998),

$$C_D \approx \frac{24}{Re} + \frac{4}{Re^{2/3}}. \quad (7)$$

So, $Re = 1$ gives $C_D = 28$. At high Reynolds numbers ($Re > 1000$), the drag coefficient is approximately constant, $C_D \approx 0.45$. This is not true if the Mach number is ≥ 1 (e.g. Henderson 1976). In such a circumstance, the drag coefficient increases. However, the effect of the Mach number is minimal for subsonic flows.

Typical cloud velocities can be estimated by various means. In the Perseus cluster, the properties of the cold gas were probed with absorption of 21 cm radio emission from a background radio source (Jaffe 1990). Typical linewidths found were 100–500 km s $^{-1}$, which greatly exceeds the expected thermal width. Similar linewidths were also found by Edge (2001) and Salomé & Combes (2003) from CO emission, and also from molecular hydrogen emission by Jaffe & Bremer (1997). These linewidths are comparable with inflow velocities in the ICM. However, this should not be taken as an indication that the clouds must be approximately co-moving with the ICM.

The Stokes number is a useful quantity to consider. It is defined as the ratio of the momentum transfer time-scale of the particle, τ_v , to the dynamic time-scale of the fluid flow around the particle. The Stokes number is

$$St = \frac{\tau_v (u - v)}{D}. \quad (8)$$

Substitution for τ_v gives

$$St = \frac{4}{3} \left(\frac{\rho_d}{\rho_c} \right) \left(\frac{1}{C_D} \right), \quad (9)$$

which is independent of the cloud size and the relative velocity. Since $\rho_d/\rho_c \gg 1/C_D$, we have $St \gg 1$. In this limit, the particle motion is not well coupled to that of the continuous phase and the two phases effectively move independently. This means that cold molecular cloud and the ICM velocities are not coupled by viscosity.

Subsonic bulk flows in the ICM are currently undetectable. Therefore, we need an alternative method to estimate the quantity $u - v$ that is important for our calculations. Thus, the Pope et al. (2008) estimate of $|u - v|$ (derived from a model of the formation of filaments due to an AGN driven outflow) may provide a reasonable estimate for the Perseus cluster.

2.2 Definitions

Before calculating the mass transfer coefficients it is necessary to define some useful parameters. The first of these is the volume-averaged density of the dispersed phase (assuming identical clouds)

$$\bar{\rho}_d = n_d m = \alpha_d \rho_d, \quad (10)$$

where n_d is the number density of clouds of volume filling factor α_d and mass density ρ_d . Similarly for the continuous phase we have

$$\bar{\rho}_c = \alpha_c \rho_c, \quad (11)$$

and the density of the mixture can be written $\rho_m = \bar{\rho}_c + \bar{\rho}_d$.

However, for ease of comparing with observations, it makes sense to write equation (10) in a different way. The volume-averaged density is simply the total mass of the dispersed phase divided by the total volume of the system

$$\bar{\rho}_d = \frac{M_d}{V}, \quad (12)$$

where V is the volume of a spherical shell, and M_d is the cold mass within the shell. Similarly for the continuous phase we have

$$\bar{\rho}_c = \frac{M_c}{V}. \quad (13)$$

3 MASS EXCHANGE

It is possible to assess the extent of the coupling between the phases by evaluating so-called ‘coupling’ parameters (Crowe et al. 1998). The continuous phase is described by the density, the temperature and the velocity field. The particle/dispersed phase is described by the concentration of particles, their size, their temperature and their velocity field. Coupling can take place through mass, momentum and energy transfer between phases. Mass coupling is the addition of mass through evaporation, or the removal of mass from the continuous phase through condensation. Momentum coupling is the result of the drag force on the dispersed and continuous phases. It can also occur due to mass transfer between the phases. Energy coupling occurs through heat transfer between the phases as well as the dissipation of kinetic energy due to drag. Thermal and kinetic energy can also be transferred between the phases by mass transfer. A quick numerical exercise demonstrates that estimates of the energy and momentum coupling, except that associated with mass exchange, are generally subject to large uncertainties, and therefore unreliable.

3.1 Definition of the mass-coupling parameter

Suppose that there are n_d clouds per unit volume in a cubic box with side X . If each cloud evaporates at a rate \dot{m} , the rate at which mass is injected by the dispersed phase in this volume is

$$\dot{M}_d = n_d X^3 \dot{m} = N \dot{m}. \quad (14)$$

The mass flux of the continuous phase through this volume is

$$\dot{M}_c \sim \bar{\rho}_c u X^2, \quad (15)$$

and the mass-coupling parameter is defined as (Crowe et al. 1998)

$$\Pi_{\text{mass}} = \frac{\dot{M}_d}{\dot{M}_c}. \quad (16)$$

If $\Pi_{\text{mass}} \ll 1$, then the effect of mass addition to the continuous phase would be insignificant. If $\Pi_{\text{mass}} \gg 1$, then the mass added to the system would dominate. The latter would be unphysical in

galaxy clusters if it occurred globally, since it would imply that the total mass of gas was not conserved. However, in a restricted region this scenario would be consistent with a fountain flow, where the clouds are replenished over and over again. In the case, where $\Pi_{\text{mass}} \sim 1$ both condensation and evaporation are important.

The mass-coupling parameter is likely to be a function of radius in galaxy clusters. Therefore, equation (16) is of little practical use, since we cannot compare like with like: the mass-flow rate of the continuous phase must be evaluated at a single radius, while the mass injected into the continuous phase corresponds to a volume.

In galaxy clusters, $\dot{M}_d(r)$ is the net rate of mass added to the flow from the clouds (evaporation – condensation), while $\dot{M}_c(r)$ is the mass flux of the hot gas. Several scenarios are possible. If there is no evaporation/condensation (i.e. no clouds at all), then $\dot{M}_c = \dot{M}_\infty$, where \dot{M}_∞ is the pure flow rate of hot material. The accretion rate of new material on to the central galaxy, \dot{M}_{gal} , is given by the value of the pure flow rate at the characteristic radius of the galaxy: $\dot{M}_\infty(r_{\text{gal}})$. If there is condensation of material out of the hot phase, but no subsequent evaporation, then $\dot{M}_c < \dot{M}_\infty$. Of course, if the clouds also accrete on to the central galaxy, \dot{M}_{gal} may still be equal to \dot{M}_∞ . A third possibility is that material evaporated from the clouds may contribute a significant fraction of \dot{M}_c , and so \dot{M}_c may exceed the actual accretion rate of ‘new’ material from infinity (i.e. $\dot{M}_c > \dot{M}_\infty$). Such a scenario would require that the mass in the clouds is predominantly from material that was previously accreted on to the central galaxy, and which has at some later time been thrown out of the central galaxy back into the ICM, perhaps through AGN activity.

Rates of mass deposition from the continuous phase to the cloud phase are inferred from X-ray data. The mass deposition in a typical cluster is consistent with a mass-flow rate that increases linearly with radius, $\dot{M}_{\text{obs}} = -\dot{M}_0(r/r_{\text{cool}})$, at $r < r_{\text{cool}}$ (e.g. Pope et al. 2006). Here \dot{M}_0 is a constant and r_{cool} is the radius at which the ICM’s radiative cooling time equals the Hubble time. If no evaporation of clouds occurred it would be reasonable to assume that the flow rate of hot gas at r_{cool} is $\dot{M}_c = \dot{M}_0$ and that the flow rate of hot gas at $r < r_{\text{cool}}$ is $\dot{M}_c = \dot{M}_0 r / r_{\text{cool}}$. Now imagine the scenario where for $r_d < r < r_{\text{cool}}$ there is pure condensation, while for $r < r_d$ material may also evaporate from clouds back into the hot phase so that there is a complex exchange of mass between the hot gas and cold clouds (i.e. condensation and evaporation, and re-condensation and re-evaporation). Much of the condensing gas at $r < r_d$ may be gas that previously evaporated from clouds recently expelled from the central galaxy in a fountain flow, or via AGN activity, for example, rather than material that fell from $r \gg r_d$. Thus, the instantaneous accretion rate on to the galaxy may exceed the long-term average [i.e. $\dot{M}_{\text{gal}} \geq \dot{M}_\infty(r_{\text{gal}})$]. Therefore, the observationally inferred mass-flow rate \dot{M}_0 may actually be an upper bound on the pure mass-flow rate, \dot{M}_∞ , with the real flow rate of ‘new’ material being $\beta \dot{M}_0$. The flow rate of new material in the hot phase is

$$\dot{M} = \beta(r) \dot{M}_0 \left(\frac{r}{r_{\text{cool}}} \right). \quad (17)$$

At $r > r_d$, $\beta(r) = 1$, while for $r < r_d$, $0 < \beta(r) < 1$. Let $\bar{\beta}$ be the average value of β integrated between $0 < r < r_d$. If there is not much recycling of material, then $\bar{\beta}$ will be close to unity. The average mass flux of new material in the hot phase at $r < r_d$ is then $\bar{\beta} \dot{M}_0 r_d / r_{\text{cool}}$. Using this and by setting $m/\dot{m} \equiv \tau_m$ as the average ablation time-scale of any cloud, we can write

$$\Pi_{\text{mass}} = \left(\frac{1}{\tau_m} \right) \left(\frac{r_{\text{cool}}}{r_d} \right) \left(\frac{M_d}{\bar{\beta} \dot{M}_0} \right). \quad (18)$$

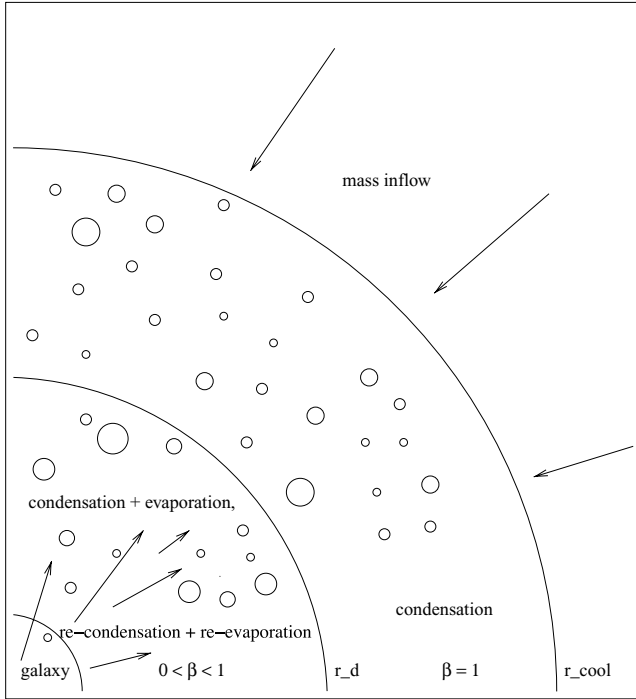


Figure 1. Schematic view of the mass cycle described in the text. Material flows inwards through r_{cool} and a fraction might condense, so, for $r_d < r < r_{\text{cool}}$ we have $\dot{M}_c(r) < \dot{M}_{\infty}$. For $r < r_d$ condensation and evaporation processes both occur as well as re-condensation and re-evaporation.

If $\bar{\beta}$ is close to unity, then Π_{mass} is small everywhere. Alternatively, if $\bar{\beta}$ is significantly less than unity, Π_{mass} could be close to unity or larger. equation (18) is written in this way because we wish to express it in terms of observable quantities, such as the total mass of cold clouds, M_d . r_d is likely to be approximately equal to the maximum distance of clouds from the central galaxy. This scenario is pictured schematically in Fig. 1.

3.2 Estimated mass-coupling parameter values

We consider the sample of seven galaxy clusters studied by Pope et al. (2006). \dot{M}_0 , r_{cool} and M_d are the mass-flow rate, the cooling radius and the mass of cloud gas, respectively. Values for them and for the mass-coupling parameter (based on the following discussion) are given in Table 1.

The rate at which mass is ablated from a cloud, \dot{m} , might be estimated by the rate at which momentum associated with the wind is transferred to the cloud, divided by a speed, $c_{s,a}$. This speed would take a value anywhere between the sound speed of material in the cloud, and the difference between the cloud speed and the average speed of material in the filament drawn from the cloud. The appropriate value of $c_{s,a}$ depends on how effective the viscous coupling (due to turbulence or any other mechanism) between the cloud material and the wind material is. The rate at which mass is lost by the cloud would then be (e.g. Pope et al. 2008)

$$\dot{m} = A\rho_c \frac{(u-v)^2}{c_{s,a}}, \quad (19)$$

where A is the cloud cross-sectional area. The ablation time-scale is

$$\tau_m \equiv \frac{m}{\dot{m}} \sim \left(\frac{\rho_d}{\rho_c} \right) \left(\frac{c_{s,a}}{u-v} \right) \left(\frac{r_0}{u-v} \right), \quad (20)$$

Table 1. Parameters for the sample of galaxy clusters used in deriving the cold gas masses and coupling parameters. Values in Columns 2 and 3 are taken from Pope et al. (2006) and references therein. The values in Column 4 are taken from Simionescu et al. (2007) for Virgo and from Edge (2001) for all others. Column 5 shows the mass-coupling parameter for a region enclosing 30 kpc around the cluster centre. The values in Column 5 could be greater if $\bar{\beta} < 1$.

Object	\dot{M}_0 ($M_{\odot} \text{ yr}^{-1}$)	r_{cool} (kpc)	M_d ($10^9 M_{\odot}$)	Π_{mass}
Virgo	1.8	35	0.5	1
Perseus	54	102	17	0.1
Hydra	14	100	<2	<0.4
A2597	59	129	8.1	0.1
A1795	18	137	<2.7	<0.4
A2199	2	113	<2.9	<3
A478	150	150	4.5	0.06

where r_0 is the initial cloud radius. We are aware of the large uncertainties in the parameters, but consider the following estimates suggestive: $r_0 \sim 50 \text{ pc}$, $\rho_d/\rho_c \sim 10^6$, $u-v \sim 10^8 \text{ cm s}^{-1}$, $c_{s,a} = 10^6 \text{ cm s}^{-1}$ and $\tau_m \sim 10^9 \text{ yr}$. Finally, we take the outer radius of cold material to be $r_d \sim 30 \text{ kpc}$. The mass-coupling parameters calculated from equation (18) are shown in Column 5 of Table 1. These values suggest that in the central regions at least, the mass coupling may be a two-way process in some clusters, and mass-loss from clouds may be significant in comparison with the mass deposited within the central regions due to the actual flow of new material. Note that the values in Table 1 are based on the highly conservative assumption that $\bar{\beta} = 1$. If $\bar{\beta} < 1$, then Π_{mass} could be significantly higher. A caveat is that the estimated value of Π_{mass} also depends on the actual mass loss rates from the clouds, which are very uncertain. Nevertheless, it seems that the mass coupling is probably an important consideration that has been omitted in numerical simulations of the ICM to date.

The mass-coupling parameter may also be interpreted in a slightly different way. The inflow of material, due to cooling, will deposit material on to the central galaxy of the cluster. Current thinking suggests that AGN activity lifts a fraction of this back into the ICM – this allows Π_{mass} to exceed unity. We can estimate the mass of cold gas in each cluster, by setting $\Pi_{\text{mass}} = 1$, and rearranging for $M_d = \bar{\beta}\tau_m(30 \text{ kpc}/r_{\text{cool}})\dot{M}_0$. These values are given in Table 2, for $\bar{\beta} = 1$. The estimated mass of cold material will be less if the ablation time-scale of the clouds is smaller than assumed.

The values in Column 2 of Table 2 compare relatively well with the observed quantities of cold gas in Column 3. This suggests that the ablation time-scale given by equation (20) may be a reasonably accurate description of the process. Furthermore, since

Table 2. Cold gas masses within 30 kpc calculated by setting $\Pi_{\text{mass}} = 1$, $\bar{\beta} = 1$ and assuming $\tau_m = 10^9 \text{ yr}$. The observed mass for Virgo is taken from Simionescu et al. (2007), all others are taken from Edge (2001).

Object	$M_d/10^9 M_{\odot}$	Observed mass/ $10^9 M_{\odot}$
Virgo	1.5	0.5
Perseus	15.9	17
Hydra	4.2	<2
A2597	13.7	8.1
A1795	3.9	<2.7
A2199	0.53	<2.9
A478	30	4.5

$\tau_m \propto (u - v)^{-2}$, it also suggests that $u - v$ cannot be too different, on average, to 10^8 cm s^{-1} . The small differences between the values may be caused by slight differences between the assumed and actual value of τ_m , by recent AGN outbursts which may have temporarily lifted significant quantities of cold material, or by differences in the cloud masses.

4 POWERING THE OPTICAL EMISSION IN GALAXY CLUSTERS

In clusters of galaxies, the momentum transfer and dissipation of energy by drag into the hot gas are generally insignificant compared to gravity and radiative cooling in the hot gas. However, energy is still dissipated by drag in significant quantities. This is interesting because the ratios of H_2 near and mid-infrared (mid-IR) to H recombination line strengths (e.g. Jaffe, Bremer & van der Werf 2001; Jaffe, Bremer & Baker 2005; Johnstone et al. 2007) are compatible with heating being due to dissipative processes (Ferland et al. 2008). It is possible that energy dissipation due to drag constitutes such a process.

We have already described how CO maps show clumpy structure (e.g. Salomé et al. 2008) and that the upper limit on the sizes of these clumps, in the Perseus cluster, is $\sim 450 \text{ pc}$. Salomé et al. (2008) suggest it is possible that these clumps are complexes of giant molecular clouds. If this is true, the limitations of spatial resolution mean it is impossible to trace the emission from a single cloud. Consequently, theoretical estimates of the emission due to physical processes involving the interaction between hot and cold phases, must be applied to a volume containing multiple clouds, rather than to an individual cloud. The total mechanical energy-injection rate required to produce filaments of average length l , with a combined mass M_d and a velocity shear along their length of Δv , is

$$\dot{E} = \delta M_d \frac{\Delta v^3}{l}, \quad (21)$$

where l is the typical length of the filaments and δ is a factor that takes into account the distribution of mass in terms of its momentum. If dM/dv and the acceleration along the filament are both constant, then $\delta = 1/12$.

Equation (21) can be written in terms of scaled quantities as

$$\dot{E} \sim 10^{41} \left(\frac{M_d}{10^9 M_\odot} \right) \left(\frac{\Delta v}{300 \text{ km s}^{-1}} \right)^3 \left(\frac{l}{15 \text{ kpc}} \right)^{-1} \text{ erg s}^{-1}. \quad (22)$$

Interestingly, equation (21) shows that the mechanical energy-injection rate is directly proportional to the total mass of the cold material. This gives a plausible theoretical explanation for the possible linear correlation between molecular gas mass and optical luminosity in figure 9 of Edge (2001).

We can use equation (22) to estimate typical energy-injection rates assuming that each of the parameters takes its typical value (e.g. $\Delta v = 300 \text{ km s}^{-1}$, as seems to be the case in the Perseus cluster) and taking the mass of cold gas from Column 3 of Table 2. Consider the Virgo cluster; we find that the typical values give $\dot{E} \sim 5 \times 10^{40} \text{ erg s}^{-1}$ compared to the observed $\sim 2 \times 10^{40} \text{ erg s}^{-1}$. In the Perseus cluster, equation (22) gives $\dot{E} \sim 2 \times 10^{42} \text{ erg s}^{-1}$ while the optical nebula around NGC 1275 actually emits $4.7 \times 10^{42} \text{ erg s}^{-1}$ in $\text{H}\alpha$ and $[\text{N II}]$. Thus, equation (22) seems to provide a reasonable explanation for the optical luminosities of both systems.

Of course, these estimates have not accounted for different average filament lengths, nor the variation in relative velocity between the hot and cold phases in the different clusters.

We can attempt to account for different average filament lengths by comparing the sizes of the optically emitting regions of the clusters. Heckman et al. (1989) give the sizes for Virgo, Perseus, Hydra-A, A2597 and A1795 which have optically emitting regions of linear diameter 14, >53 , 13, 22 and 61 kpc, respectively. We note that the optically emitting region of A1795 is dominated by a single filament, so that the remainder of the optical emission is probably contained within $\sim 15 \text{ kpc}$, which provides a more realistic estimate. Heckman (1981) also gives the size of the optical region in Perseus as $\sim 60 \text{ kpc}$. Using these values, we can estimate the average length of a filament by assuming it is a constant fraction of the total diameter of the optically emitting region, for example 0.25. This gives average filament lengths of ~ 4 , 15, 3, 6 and 4 kpc for the filaments in Virgo, Perseus, Hydra-A, A2597 and A1795, respectively. The average filament lengths of the clusters that we do not have diameters for (A2199 and A478) will be taken to be 5 kpc, which is representative of the sample.

For the velocity shears, we have an estimate of $\Delta v \sim 300 \text{ km s}^{-1}$ along the length of the filaments in Perseus from Hatch et al. (2006), but we do not have similarly detailed observations for any other clusters in the sample. In addition, linewidths at other frequencies do not give an indication of a single well-defined value of Δv in each cluster. Therefore, we will assume a canonical value for Δv as 300 km s^{-1} which we know applies adequately in the Perseus cluster. This will then be scaled to each cluster by multiplying it by the ratio of the cluster gravitational potential at the maximum extent of the optically emitting region to that of the Perseus cluster. That is, the value of Δv that we will use for a given cluster will be $300 \text{ km s}^{-1} \times (\phi_{\text{cluster}}/\phi_{\text{perseus}})^{1/2}$.¹ Such an approach is ad hoc, but does attempt to account for the different environments. Henceforth, we will refer to this multiplicative factor by $f \equiv (\phi_{\text{cluster}}/\phi_{\text{perseus}})^{1/2}$, see Table 3. The gravitational potentials are estimated from the temperature and density profiles for each cluster, with the assumption that the gas is in hydrostatic equilibrium. Fits to the temperature and density data are taken from Pope et al. (2006) and they were numerically integrated from the origin to obtain the gravitational potential at the edge of the optically emitting region. It was not possible to determine a gravitational potential for A2199 due to the power-law fits to the data. Consequently, we assigned $f = 1$ for this object.

These scalings have been applied to the sample of clusters used in Pope et al. (2006) and Pope et al. (2007). The optical luminosities for this sample are taken from Crawford et al. (1999) and Heckman et al. (1989). As can be seen from Table 3, the expected energy-injection rates are generally comparable with the $\text{H}\alpha + [\text{N II}]$ luminosities.

Fig. 2 demonstrates a relatively good match between the mechanical energy-injection rate, and the combined $[\text{N II}] + \text{H}\alpha$ optical luminosity. In fact, the best fit shows that $f \times 400 \text{ km s}^{-1}$ provides a better description of the velocities. This, particularly the scaling, agrees with the findings of Edge (2001). It therefore seems possible that the dissipation of mechanical energy may be evident in the $[\text{N II}]$ line emission, which traces the heating rate, while there may be an ionizing source which produces the $\text{H}\alpha$ emission. Regardless of this, the general conclusion that optical emission increases with mechanical power is consistent with Ferland et al. (2008) who found that the H_2 to H recombination line ratios are compatible with dissipative heating.

It is worthwhile pointing out that our estimate for A1795 falls below the observed optical luminosity. This is probably because the assumed velocity is a conservative estimate given the current likely

¹ The square root occurs because $v \sim \phi^{1/2}$.

Table 3. Mechanical energy-injection rates calculated with equation (23) using the observed cold gas masses (in table 1). In Column 2, we list the average filament lengths derived from the size of the optically emitting region. The gravitational potential f factors are given in Column 3. The estimated optical luminosities are shown in Column 4, the observed optical luminosities are in Column 5, the X-ray luminosities in Column 6 are taken from Pope et al. (2006) and references therein, and the references are shown in Column 7. Reference 3 is Heckman et al. (1989); reference 4 is Crawford et al. (1999). Using the [N II] fluxes given by Crawford et al. (1999), we have calculated $L(\text{H}\alpha + [\text{N II}])$ rather than $L(\text{H}\alpha)$. The luminosities from reference 3 are the sum of the $\text{H}\alpha$ and [N II] luminosities. Heckman et al. (1989) did not give uncertainties.

Object	l	f	$\dot{E}/10^{40} \text{ erg s}^{-1}$	$L(\text{H}\alpha + [\text{N II}])/10^{40} \text{ erg s}^{-1}$	$L_X/10^{42} \text{ erg s}^{-1}$	Ref
Virgo	4	0.8	9	1.9	9.8	3
Perseus	15	1	200	470	670	3
Hydra	3	0.8	<51	15	250	3
A2597	6	0.8	210	270	430	3
A1795	4	0.4	<8	82	490	3
A2199	5	1	<90	5.9	150	4
A478	5	0.5	17	22.7	1220	4

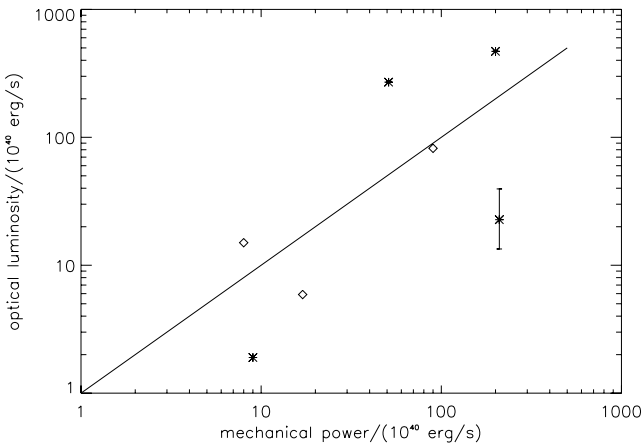


Figure 2. Comparison between the mechanical energy-injection rate and $\text{H}\alpha + [\text{N II}]$ luminosity. The diamonds show the objects for which the \dot{E} is an upper limit. As a result, we may expect these points to move to the left-hand side if the mass of cold gas is less than the upper limit. The stars denote the remainder of the sample. Ideally, we would compare the mechanical energy-injection rate to $L([\text{N II}])$, but this is not possible since we do not have $L([\text{N II}])$ values for the objects in the Heckman et al. (1989) sample. The line indicates where the optical luminosity is equal to the mechanical energy-injection rate. Note that alterations in the normalization could be achieved by employing a different relative velocity between the phases. Uncertainties are shown for A478, by Crawford et al. (1999). The other measurements are taken from Heckman et al. (1989) who did not provide uncertainties.

state of the system. The AGN has been recently active and indeed has injected more energy than any of the others in the sample, save for the one in Hydra-A, which is a well-known powerful AGN, so a fast outflow would be expected in the central regions. In addition, this system would only requires $\Delta v \sim 300 \text{ km s}^{-1}$ to account for the optical emission, so it seems more than likely that mechanical energy can account for the optical emission. A similar explanation also accounts for the apparent deficit in the Perseus cluster.

The question of why some clusters are brighter than others in their optical emission remains. The mechanical energy-injection rate seems to be proportional to the total mass of cold gas so that clusters with more cold gas are likely to exhibit more optical emis-

sion. This leads to the question: why is there more cold gas in some clusters than others? The mass of cold gas is related to the mass-flow rate, which is, in turn, related to the balance between heating and cooling in the cluster. There may also be an additional component of material thrown up from the central galaxy. It is important to note the strong effect of the velocity difference between the phases. This is again likely to be related to AGN activity, so that the optical luminosity in clusters with AGN is likely to be larger than expected.

4.1 IR emission

There is also significant IR emission from the molecular gas near cluster centres. Jaffe et al. (2005) quote luminosities of $\sim 10^{42} \text{ erg s}^{-1}$ for the $\text{H}_2(1-0) \text{ S}(1)$ line in A2597 and suggest that this comprises roughly 1–2 per cent of the total molecular near-infrared (NIR) emission due to H_2 . This would imply a total NIR luminosity of $10^{44} \text{ erg s}^{-1}$ which greatly exceeds the optical luminosity for A2597. Jaffe & Bremer (1997) also give luminosities of $\sim 10^{40} \text{ erg s}^{-1}$ and $\sim 10^{41} \text{ erg s}^{-1}$ for the $\text{H}_2(1-0) \text{ S}(1)$ line in A478 and Hydra-A, respectively. This implies total NIR luminosities of 10^{42} – $10^{43} \text{ erg s}^{-1}$, respectively. Such values are comparable with the optical luminosities of the systems, although not in the case of A2597. However, it is still feasible that the injection of mechanical energy can also account for the NIR emission. To obtain a mechanical energy-injection rate of $\sim 10^{44} \text{ erg s}^{-1}$ in A2597 requires $\Delta v \sim 700$ – 800 km s^{-1} . Such values are comparatively large, but probably close to a Mach number of unity for the hot gas in the cluster centre and are therefore perfectly permissible. Furthermore, A2597 shows evidence for a recent, moderately powerful AGN outburst (Bîrzan et al. 2004); therefore, transonic velocities close to the cluster centre are to be expected. The same is true for Hydra-A, which also shows strong NIR emission and currently hosts a strong AGN outburst.

5 DISCUSSION AND SUMMARY

The effect of mass injection into a diffuse flow in a gravitational potential was investigated by Pittard et al. (2004) using 1D hydrodynamical simulations. Regularly spaced shock-like structures were obtained under some conditions, which could provide an alternative explanation for the structures generally believed to be AGN-driven shocks. Other simulations revealed a differential

luminosity function which resembled those deduced from observations (e.g. Peterson et al. 2003). However, along with these successes are a number of areas for concern. First, the amount of material that was added was not related to the mass deposition rate (expected from cooling), and eventually dominated the total gas mass in the system. However, this is less of a problem if the flows are fountain-like. Secondly, the resulting X-ray luminosity was far too centrally peaked. This may be related to the form of the gravitational potential used, and it would be worth revisiting the model, to see what the effect of a realistic cluster potential, and realistic mass transfer rates, would have. It may also be necessary to include thermal conduction as well, to see whether these structures would be smoothed out by the same process that evaporates the clouds.

Our analysis in the current work indicates that the rate of mechanical energy-injection is comparable with the optical luminosity in the sample. Since the [N II] emission is a tracer of the heating rate of the nebular gas, it seems possible that the observed emission is indeed powered by mechanical energy injection. Furthermore, given that the energy dissipation rate is proportional to $(u - v)^3$. It is not surprising that optical emission occurs frequently in cool-core clusters, since AGN are frequently found in such environments. That is not to say that radiation from the AGN is responsible for the emission, but that AGN-induced bulk motions in the ICM are likely to cause significant interactions with the cold material in the central regions of clusters which may be evident through the optical emission. It may also be revealing that optical emission in clusters with AGN is generally more luminous than would be predicted. It is also possible that a component of the $H\alpha$ is due to the same process, though photoionization also plays a role. As we have already stated, it is also possible that mechanical energy also powers the NIR emission. Again, prominent NIR emission seems to occur in systems with powerful AGN. As a result, it is possible that the presence of cold material may automatically lead to physical processes which power the observed optical and IR emission. In this figure, the injection of energy will necessarily be relatively constant and distributed, in accordance with observational constraints.

This work suggests that there are plausible theoretical reasons which could explain the rough proportionality between the total optical luminosity and the total mass of cold material observed by Edge (2001). The total cold mass is likely to depend on the heating/cooling balance in the cluster centres, thus providing us important information on the deviation from equilibrium between these processes.

Our numerical simulations (Pope et al. 2008) indicate that, if formed by outflows, filaments can only be formed if there is a sufficiently fast wind ($> \text{few} \times 10^7 \text{ cm s}^{-1}$). Without this wind, any cold, dense material stripped from a cloud would sink towards the cluster centre with the cloud, rather than forming a long tail behind the cloud. Thus, a slower wind may lead to amorphous optical emission, without filaments. Consequently, the morphology of the optically emitting region is likely to be strongly dependent on the magnitude of the relative motion between the ICM and the cold phase.

To summarize, we have two main points.

(i) There is enough cold gas within the central 30 kpc, or so, of most galaxy clusters for its evaporation to contribute significantly to the density of the hot gas in this region. Therefore, to obtain a more complete understanding of the behaviour of the ICM this effect should be included in future numerical simulations.

(ii) In general, it seems that the mechanical energy or momentum injection will not affect the thermal structure of the hot phase, but

it may account for, at least, the [N II] component of the optical emission of the filaments and the NIR emission. Under exceptional circumstances this process could also alter the flow dynamics of the ICM and account for some heating in the central regions of clusters.

ACKNOWLEDGMENTS

We wish to thank Nina Hatch and Paul Nulsen for informative discussions and the referee, Walter Jaffe, for very helpful comments that improved this work. JMP thanks the Royal Society for funding. This work was funded in part by STFC.

REFERENCES

- Birzan L., Rafferty D. A., McNamara B. R., Wise M. W., Nulsen P. E. J., 2004, *ApJ*, 607, 800
- Boehringer H., Fabian A. C., 1989, *MNRAS*, 237, 1147
- Crawford C. S., Allen S. W., Ebeling H., Edge A. C., Fabian A. C., 1999, *MNRAS*, 306, 857
- Crawford C. S., Fabian A. C., 1992, *MNRAS*, 259, 265
- Crowe C., Sommerfeld S., Tsuji Y., 1998, *Multiphase Flows With Droplets And Particles*. CRC Press, London
- Daines S. J., Fabian A. C., Thomas P. A., 1994, *MNRAS*, 268, 1060
- Donahue M., Voit G. M., 1991, *ApJ*, 381, 361
- Donahue M., Mack J., Voit G. M., Sparks W., Elston R., Maloney P. R., 2000, *ApJ*, 545, 670
- Edge A. C., 2001, *MNRAS*, 328, 762
- Ferland G. J., Fabian A. C., Hatch N. A., Johnstone R. M., Porter R. L., van Hoof P. A. M., Williams R. J. R., 2008, *MNRAS*, 386, L72
- Field G. B., 1965, *ApJ*, 142, 531
- Hatch N. A., Crawford C. S., Johnstone R. M., Fabian A. C., 2006, *MNRAS*, 367, 433
- Hatch N. A., Crawford C. S., Fabian A. C., 2007, *MNRAS*, 380, 33
- Heckman T. M., 1981, *ApJ*, 250, L59
- Heckman T. M., Baum S. A., van Breugel W. J. M., McCarthy P., 1989, *ApJ*, 338, 48
- Henderson C. B., 1976, *AIAA J.*, 14, 707
- Jaffe W., 1990, *A&A*, 240, 254
- Jaffe W., Bremer M. N., 1997, *MNRAS*, 284, L1
- Jaffe W., Bremer M. N., van der Werf P. P., 2001, *MNRAS*, 324, 443
- Jaffe W., Bremer M. N., Baker K., 2005, *MNRAS*, 360, 748
- Johnstone R. M., Hatch N. A., Ferland G. J., Fabian A. C., Crawford C. S., Wilman R. J., 2007, *MNRAS*, 382, 1246
- Loewenstein M., Fabian A. C., 1990, *MNRAS*, 242, 120
- McKee C. F., Cowie L. L., 1977, *ApJ*, 215, 213
- Peterson J. R., Kahn S. M., Paerels F. B. S., Kaastra J. S., Tamura T., Bleeker J. A. M., Ferrigno C., Jernigan J. G., 2003, *ApJ*, 590, 207
- Pittard J. M., Hartquist T. W., Ashmore I., Byfield A., Dyson J. E., Falle S. A. E. G., 2004, *A&A*, 414, 399
- Pope E., Kaiser C., Pavlovski G., Fangohr H., 2007, preprint (astro-ph/0702683)
- Pope E. C. D., Pavlovski G., Kaiser C. R., Fangohr H., 2006, *MNRAS*, 367, 1121
- Pope E. C. D., Pittard J. M., Hartquist T. W., Falle S. A. E. G., 2008, *MNRAS*, 385, 1779
- Ruszkowski M., Enßlin T. A., Brüggem M., Heinz S., Pfrommer C., 2007, *MNRAS*, 378, 662
- Salomé P., Combes F., 2003, *A&A*, 412, 657
- Salomé P., Revaz Y., Combes F., Pety J., Downes D., Edge A. C., Fabian A. C., 2008, *A&A*, 483, 793
- Simionescu A., Böhringer H., Brüggem M., Finoguenov A., 2007, *A&A*, 465, 749

This paper has been typeset from a $\text{\TeX}/\text{\LaTeX}$ file prepared by the author.